Roller Drawing of Polyoxymethylene

AKIRA KAITO, KAZUO NAKAYAMA, and HISAAKI KANETSUNA,
Research Institute for Polymers and Textiles, 1-1-4, Yatabe-Higashi, Tsukuba, Ibaraki 305, Japan

Synopsis

The roller drawing of polyoxymethylene (POM) sheets was carried out in the temperature range of 140–157°C. The mechanical properties, the molecular orientation, and the microstructure of the roller-drawn POM sheets were investigated by means of tensile test, dynamic viscoelasticity, wide-angle X-ray diffraction, small-angle X-ray scattering, visible dichroic spectrum, electron microscopy, and so on. The Young's modulus and the tensile strength increased with increasing draw ratio up to draw ratio, λ of 14–15. The improvement of the mechanical properties is concerned with structural changes, such as the increase in orientation function in the crystalline and amorphous regions and the formation of taut tie molecules and crystalline bridges in the intercrystallite and interfibrillar regions. In the higher draw ratio range ($\lambda > 15$), the increase in Young's modulus and tensile strength was restricted by the formation of interfibrillar microvoids.

INTRODUCTION

Plastic deformation of thermoplastic polymers has been extensively studied because of its capability of producing high-strength and high-modulus polymeric materials. The improvement of the mechanical properties is believed to result from alignment of molecular chains in the mechanical direction and changes in microstructure. A polyoxymethylene (POM) fiber with tensile modulus of 35 GPa was produced by two-stage drawing in the solid state.[1] The structure of the drawn POM fiber was interpreted as approaching a continuous crystalline matrix in the drawing process.[1] A POM tape with tensile modulus of 39.5 GPa was obtained by drawing a dumb-bell-shaped sample.[2] Cold rolling and hot rolling were applied to modify the mechanical properties of POM sheets.[3,4] Highly oriented POM rods with high axial Young's moduli were produced by hydrostatic extrusion[5,6] and by die drawing.[7,8] Recently, POM rods and tubes with modulus up to 60 GPa were produced by drawing under dielectric heating,[9,10] which is able to heat selectively the noncrystalline region more intensely than the crystalline region.

On the other hand, we recently examined the roller drawing of high-density polyethylene,[11] polypropylene,[12] and ultrahigh-molecular weight polyethylene[13] sheets, and showed the process useful for the production of high-modulus polymer sheets. In this method, the polymer sheets were uniaxially stretched to a high extension by drawing through a pair of heated rollers.

In this work, we applied the roller-drawing technique to producing high-modulus POM sheets and studied the mechanical properties, molecular orientation, and microstructure of the roller-drawn POM sheets.

Journal of Applied Polymer Science, Vol. 32, 3499–3513 (1986)
 CCC 0021-8995/86/023499-15$04.00

EXPERIMENTAL

Sample Preparation

The samples used in this work were POM homopolymer, Tenac 5010 (Asahi Chemical Industry Co., Ltd.) and POM copolymer, Duracon M 25 (Polyplastics Co., Ltd.). Sheets 1–2 mm thick and 10–40 mm wide were used for the roller-drawing experiment.

The apparatus for roller-drawing was reported in the previous papers.[11,12] A pair of heated rollers with a diameter of 50 mm were attached to the upper side of the crosshead of a tensile testing machine, Tensilon UTM-10T (Toyo Baldwin Co., Ltd.). An original POM sheet, preheated between hot plates, was drawn through the rollers by lowering the crosshead of the tensile testing machine. The roller drawing was carried out at draw velocity, v_d of 10-50 mm/min and at roller temperature, T_r of 140–157°C. Draw ratio was controlled by changing roller spacing. The ratio of roller spacing to original sheet thickness was varied in the range 0.4–0.09.

Characterization

Tensile tests were carried out at 23±1°C and 50±2% of relative humidity using a tensile testing machine, Tensilon UTM-III-100 (Toyo Baldwin Co., Ltd.), with a gauge length of 12.5 mm and a tensile rate of 4 mm/min.

The dynamic viscoelastic properties were measured at 11 Hz with a dynamic viscoelastometer, Rheovibron DDV-II-EA (Toyo Baldwin Co., Ltd.).

Wide-angle X-ray diffraction (WAXD) patterns were taken with a plate camera. Ni-filtered Cu-Kα radiation (40 kV, 30 mA) produced by a Geiger Flex XGC-20 (Rigaku Denki Co., Ltd.) was used. The WAXD intensity profiles were measured using a scintillation counter and a pulse height analyzer.

WAXD pole figures were measured by employing both transmission and reflection techniques. The WAXD intensity was corrected for background and absorption.

The degree of orientation of the crystal a- and c-axes was calculated from WAXD intensity distribution of the (100) reflection using Hermans orientation function.[14]

The crystallite size normal to the (100) plane, D_{100} was calculated from the integrated line width of the (100) reflection using a Scherrer equation,[15] while the crystallite size, D_{001} and the relative fluctuation of (001) planes were obtained from the integrated line widths of the (009) and (0018) reflections in terms of a Hosemann equation.[16] The WAXD intensity profiles were corrected for Kα doublet and instrumental broadening.

The visible dichroism of samples dyed with C. I. Disperse Yellow 7 was used for evaluating the orientation function of the amorphous region.[17] The deviation from symmetric uniaxial orientation was examined by film-tilting measurements.[18]

Small-angle X-ray scattering (SAXS) patterns were taken with a vacuum camera using Ni-filtered Cu Kα radiation (50 kV, 100 mA) produced by a Rota Flex RU-200 (Rigaku Denki Co., Ltd.). In order to evaluate the long

period, the SAXS intensity profiles were measured using a scintillation counter.

The weight fraction crystallinity was calculated from the heat of fusion measured with a Perkin Elmer DSC-2 differential scanning calorimeter. The value of 75.5 cal/g was used for the heat of fusion of POM crystals.[19] Density was measured with a carbon-tetrachloride-toluene-density gradient column at 25°C. For opaque samples, the volume fraction of internal microvoids was evaluated from the measured density and the crystallinity calculated from heat of fusion. For transparent samples in which the microvoid content was negligibly small, the weight fraction crystallinity was also calculated from density assuming the densities of the crystalline and amorphous phases to be 1.492 g/cm^3 and 1.320 g/cm^3, respectively.[20,21]

The roller-drawn sheets were fractured along the draw direction in liquid nitrogen. The fracture surface was coated with gold and examined with a model S-500 scanning electron microscope (Hitachi, Ltd.).

RESULTS AND DISCUSSION

Appearance and Sample Size of Roller-Drawn Sheets

Roller-drawing produced POM sheets with smooth surfaces and uniform thickness. The roller-drawn POM homopolymer sheet with draw ratio, λ of 4.5 was opaque, while the roller-drawn POM copolymer sheet of similar draw ratio ($\lambda = 4.1$) was translucent. The roller-drawn homopolymer and copolymer sheets were transparent in the draw ratio range of 7–14 and became opaque in the higher draw ratio range ($\lambda = 15$–20).

The width of the sheets decreased by the roller drawing. The degree of width contraction was 5–20% and decreased with increasing width of the original sheet.

Draw ratio and thickness reduction ratio increased as roller spacing was narrowed. The ratio of thickness of a drawn sheet to roller spacing lay in the range of 0.63–0.90 and increased with narrowing roller spacing. Roller drawing consists of two deformation processes: isothermal thickness reduction between rollers and nonisothermal drawing in the post roller zone. The former was a major deformation process in the roller drawing of POM sheets.

Effect of Roller Temperature and Sample Size on Maximum Draw Ratio

Table I shows the effect of roller temperature and sample size on maximum draw ratio, λ_{max}. In this work, draw ratio is defined by the ratio of length after and before roller drawing. The maximum draw ratio was almost independent of original sheet thickness, but much decreased with increasing width of original sheets. In the roller drawing to high draw ratio, a wider sheet tore more easily accompanied by crack generation in the draw direction. The value of λ_{max} slightly increased as T_r rose.

TABLE I
Effect of Sample Size and Roller Temperature on Maximum Draw Ration, λ_{max} and Tensile Properties

Grade	T_r(°C)	Width[a] (mm)	Thickness[a] (mm)	λ_{max}	Young's modulus (GPa)	Tensile strength (GPa)
Homopolymer	157	10	1	20.0	25.6	0.763
	157	10	2	21.5	23.1	0.738
	157	20	1	14.3	24.9	1.084
	157	20	2	14.3	22.6	1.045
	157	40	1	9.2	15.7	0.805
	157	40	2	9.2	12.0	0.823
	140	20	1	11.1	18.8	0.909
Copolymer	150	10	1	19.6	19.1	0.847
	150	20	1	13.0	14.1	0.926
	150	40	1	9.6	10.2	0.761
	140	20	1	11.6	14.3	0.890

[a] Sample size of original POM sheets.

We hereafter report the mechanical properties and microstructure of the roller-drawn sheet whose original sheet thickness and width are 1 mm and 10–20 mm, respectively.

Tensile Properties

The tensile properties of the roller-drawn POM sheets are shown in Figure 1 as functions of draw ratio. A yield point was observed in the stress–strain curve of original POM sheets, while roller-drawn POM sheets uniformly deformed without showing a yield point during tensile tests. The Young's

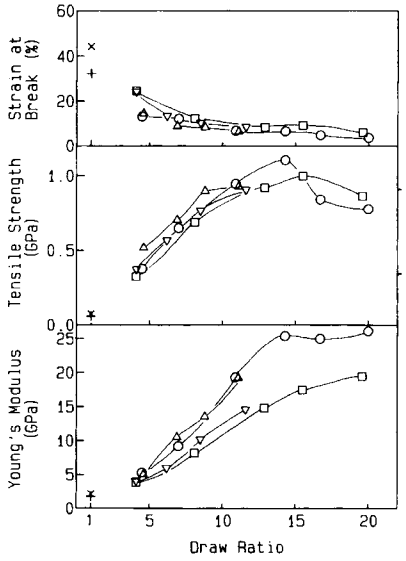

Fig. 1. Tensile properties vs. draw ratio: (△) homopolymer, T_r = 140°C; (○) homopolymer, T_r = 157°C; (×) original homopolymer sheet; (▽) copolymer, T_r = 140°C; (□) copolymer, T_r = 150°C; (+) original copolymer sheet.

modulus and the tensile strength increased with increasing draw ratio in the draw ratio range of $\lambda < 14$. The increase in the Young's modulus was suppressed and the tensile strength decreased with increasing draw ratio in the higher draw ratio range ($\lambda > 14$). Strain at break decreased rapidly at lower draw ratio and approached a constant value at $\lambda = 10$. At the same draw ratio, the Young's modulus of roller-drawn homopolymer sheets was higher than that of the roller-drawn copolymer sheets.

The tensile properties of the POM sheets roller drawn to λ_{max} are presented in Table I. At the same draw ratio and sample width, the Young's modulus at λ_{max} slightly decreased by the increase in original sheet thickness.

Dynamic Viscoelastic Properties

Figure 2 shows temperature dependence of dynamic viscoelastic properties of the roller-drawn homopolymer sheets. The tan δ peak located around −60°C (γ-dispersion peak) is associated with main chain micro-Brownian motion in the amorphous region. The tan δ peak of the roller-drawn homopolymer sheet of $\lambda = 4.5$ was higher than that of the original sheet, which is attributable mainly to the increase in the degree of amorphous orientation. With further increasing draw ratio, the tan δ peak became smaller, suggesting that the molecular motion of amorphous chains is restricted in the highly drawn sheets. The dynamic storage modulus, E' much decreased with the rise of temperature in the γ-dispersion region. The fall in E' in the γ-dispersion region was highest at $\lambda = 4.5$, and decreased with increasing draw ratio.

The tan δ peak observed around 100–170°C (α-dispersion peak) is associated with the molecular motion in the crystalline region. The roller-drawn

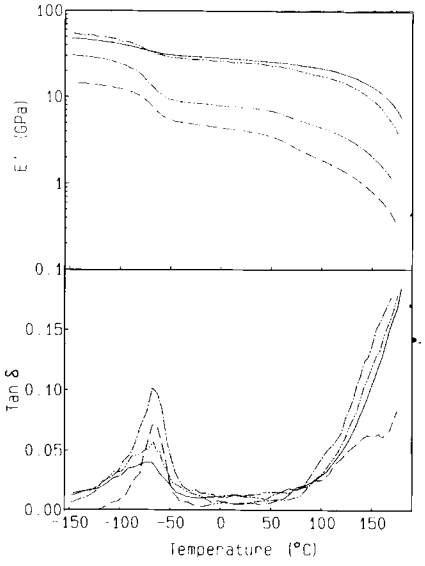

Fig. 2. Dynamic viscoelastic properties of roller-drawn POM homopolymer sheets: (- - -) original homopolymer sheet; (- • - • -)T_r = 157°C, λ = 4.5; (- ••- ••-) T_r = 157°C, λ = 13.6; (——) T_r = 157°C, λ = 20.0.

sheets showed the higher tan δ peak in the α-dispersion region than the original sheet. The increase of the tan δ peak might be attributed to the increase in the degree of crystal orientation and the degree of crystallinity.

Wide-Angle X-Ray Diffraction

The WAXD patterns of the roller-drawn homopolymer sheets are given in Figure 3. Carazzolo and Mammi reported two crystalline forms of POM, hexagonal unit cell with 9/5 helix and orthorhombic unit cell with 2/1 helix.[22,23] The WAXD pattern shows that only the hexagonal unit cell with 9/5 helix is present in the roller-drawn POM sheets. In the roller-drawn sheet of $\lambda = 4.5$, the (100) reflection consisted of a strong maximum on the equator and a weak ring. There are two modes of orientation of the crystal a-axis: one highly oriented perpendicular to the draw direction and another almost randomly distributed. The intensity of the ring pattern much decreased at $\lambda = 7.0$ and almost disappeared at $\lambda = 14.3$.

The WAXD intensity profile on the meridian is shown in Figure 4. We observed the intense (009) and (0018) reflections and the weak (005) reflection. Uchida and Tadokoro investigated the detailed molecular structure in orthorhombic POM with 9/5 helix.[24] According to their analysis, the (00l) reflection is allowed in 9/5 helix only when l is a multiple of nine. Saruyama et al. observed forbidden reflections on the meridian in drawn and drawn/annealed POM and demonstrated the presence of two kinds of hexagonal POM crystals: one exhibiting the (003), (0015), and (0021) reflections and another generating the (005) and (0013) reflections.[25] The forbidden reflections were interpreted as arising from periodic distortion of the molecular conformation from the uniform 9/5 helix.[25] In the roller-drawn sheets of lower draw ratio ($\lambda \leqq 4.5$), the (005) reflection might be hidden behind the stronger (100) reflection, while the roller-drawn sheets with higher draw ratio ($\lambda > 6$) exhibited the clearly resolved (005) reflection. The ratio of intensity of the (005) to (009) reflections was almost independent of draw ratio, roller temperature, and sample grade, and lay in the range 0.016–0.019. This result suggests that the amplitude of the conformational

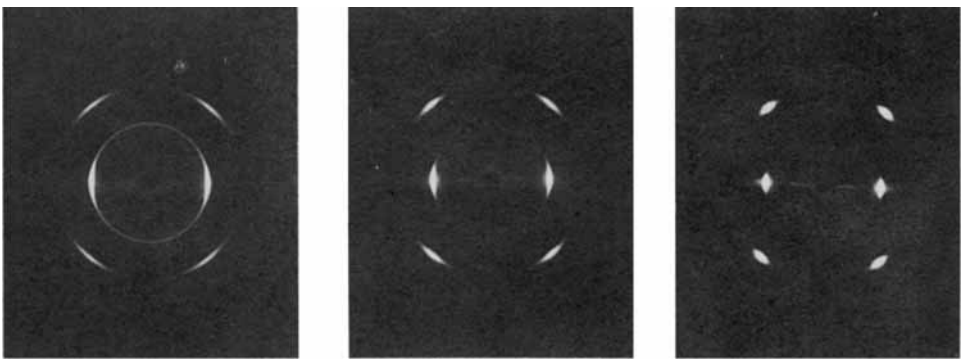

λ : 4.5 7.0 14.3

Fig. 3. Wide-angle X-ray diffraction patterns of roller-drawn POM homopolymer sheets (T_r = 157°C): draw direction is vertical.

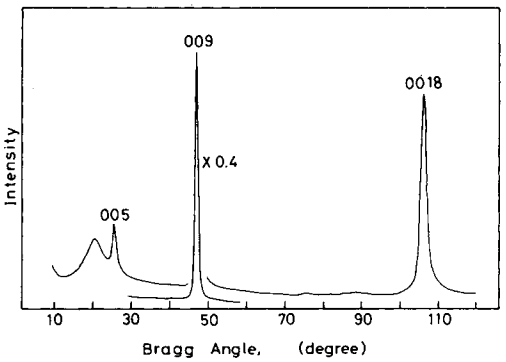

Fig. 4. WAXD intensity distribution of the roller-drawn POM homopolymer sheet (T_r = 157°C, λ = 14.3) on the meridian.

distortion is almost unaffected by draw ratio, roller temperature, and sample grade.

Pole Figures

The WAXD pole figures of the roller-drawn homopolymer sheets are shown in Figures 5 and 6. The principal axes of the sheets are labeled DD (draw direction), TD (traverse direction), and ND (normal direction). The intensity contour labeled 1, 2,..., and 9 represents 10, 20,..., and 90% of the maximum intensity, respectively. The 009 pole figure was accompanied by the poles of (200), (201), and (115) reflections. However, they were separated from the 009 pole maximum by more than 57°, and were not overlapped with the 009 pole in the oriented sample. The 100 pole was distributed in

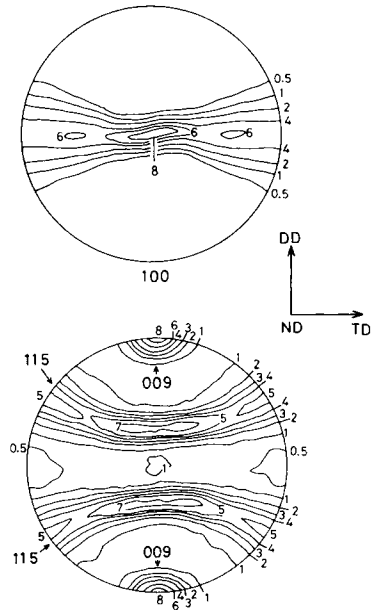

Fig. 5. 100 and 009 pole figures of the roller-drawn POM homopolymer sheet (T_r = 157°C, λ = 4.5).

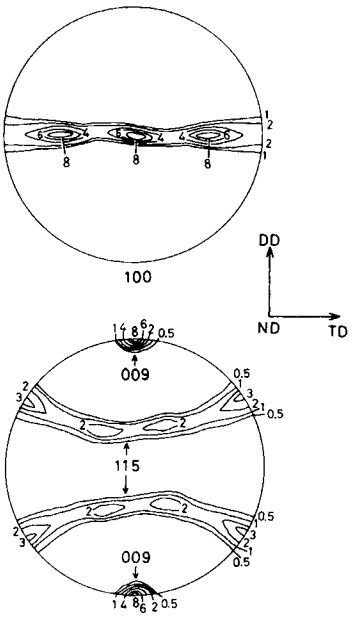

Fig. 6. 100 and 009 pole figures of the roller-drawn POM homopolymer sheet (T_r = 157°C, λ = 14.3).

the ND-TD line and showed three maxima at ND and at 60° from ND to TD. The 009 pole exhibited symmetric uniaxial orientation to DD. The principal feature of the crystal orientation is the c-axis orientation to DD and the (100) alignment in the sheet plane. Crystal orientation was much improved by the increase in draw ratio.

We also measured the (100) and (009) pole figures of roller-drawn copolymer sheets and found that the pole figures of copolymer sheets had a resemblance to those of homopolymer sheets.

Orientation Functions

In this work, orientation of molecular chains is expressed using two orientation functions, f_θ and f_ϕ.

$$f_\theta = (3\langle\cos^2\theta\rangle_{av} - 1)/2 \tag{1}$$

$$f_\phi = \langle\cos 2\phi \sin^2\theta\rangle_{av}/\langle\sin^2\theta\rangle_{av} \tag{2}$$

The angle, θ is measured between the chain axis and DD, and ϕ is the angle between the projection of the chain axis on the ND-TD plane and TD. If the molecular chains perfectly orient to DD, $f_\theta = 1$. The complete orientation to TD and ND is represented by ($f_\theta = -0.5, f_\phi = 1$) and ($f_\theta = -0.5$, $f_\phi = -1$), respectively.

It is evident from the shape of the 009 pole figure, that the crystal c-axis of the roller-drawn POM sheets is uniaxially oriented in the draw direction ($f_\phi = 0$). Orientation functions of the crystal c-axis and the amorphous molecular chains are shown in Figure 7. The orientation function, f_θ of the

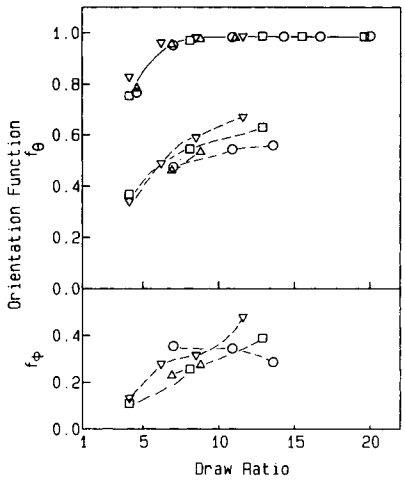

Fig. 7. Orientation functions in crystalline (——) and amorphous (- - -) regions vs. draw ratio: (△) homopolymer, T_r = 140°C; (○) homopolymer, T_r = 157°C; (▽) copolymer, T_r = 140°C; (□) copolymer, T_r = 150°C.

crystal c-axis increased with increasing draw ratio in the lower draw ratio range ($\lambda < 8$), and reached a constant value (f_θ = 0.97-0.99) above $\lambda = 8$.

The amorphous orientation functions were evaluated from visible dichroic spectra of Disperse Yellow 7, which was dissolved in the roller-drawn POM sheets. The value of f_ϕ was obtained by the film-tilting measurements.[18] The amorphous orientation function could not be measured for the highly drawn POM sheets ($\lambda > 14$) because of decrease in transparency. The value of f_θ in the amorphous region increased with increasing draw ratio even in the draw ratio range in which the crystal orientation was saturated. The roller-drawn copolymer sheets showed slightly higher degree of amorphous orientation than the roller-drawn homopolymer sheets. The value of f_ϕ was positive and slightly increased with increasing draw ratio. The amorphous orientation deviates considerably from symmetric uniaxial orientation in a way that molecular chains tend to orient to TD rather than to ND. This result is in contrast to the case of roller-drawn high-density polyethylene and polypropylene sheets, in which the deviation from uniaxial orientation is quite small (f_ϕ = 0.0 – 0.2).[26]

Small-Angle X-Ray Scattering

Figure 8 shows SAXS patterns of the roller-drawn homopolymer sheets with incident X-ray beam parallel to ND and TD (hereafter called ND-pattern and TD-pattern, respectively). A two-point SAXS was observed on the meridian in the TD- and ND-patterns of the homopolymer sheets of λ = 4.5 and λ = 7.0. The crystalline and amorphous regions are stacked alternately along DD to form the periodic two-phase structure in this draw ratio range. The intensity of the two-point SAXS much decreased with increasing draw ratio and disappeared above λ = 14.3. In the roller-drawn sheets of λ = 4.5, 14.3, and 20.0, we observed equatorial scattering which is originated from microvoids. The intensity of the microvoid scattering much increased at higher draw ratio.

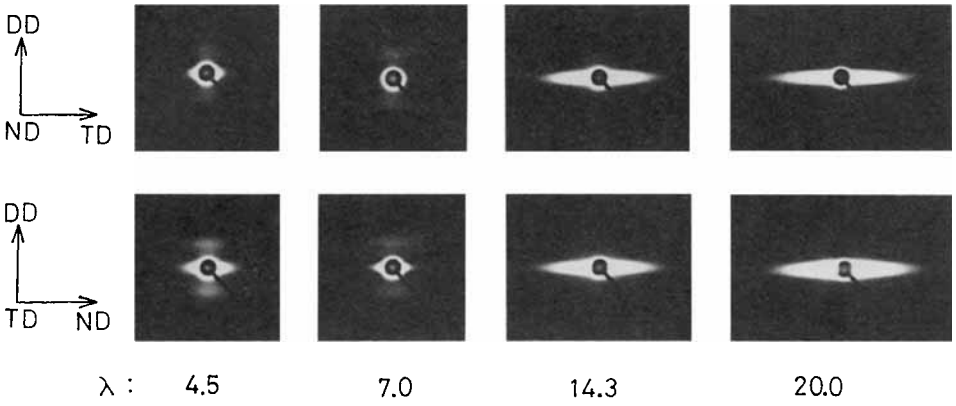

Fig. 8. SAXS patterns of roller-drawn POM homopolymer sheets (T_r = 157°C).

SAXS patterns of the roller-drawn copolymer sheets are shown in Figure 9. The SAXS pattern of the roller-drawn copolymer sheets exhibited the similar draw ratio dependence to that of the homopolymer sheets as a whole. The difference was, however, found in the TD-pattern at the lowest draw ratio (λ = 4.1 and 4.5). Instead of the equatorial microvoid scattering of the homopolymer sheet (λ = 4.5), the copolymer sheet (λ = 4.1) gave rise to diffuse four-point SAXS in the TD-pattern.

Crystallinity and Void Content

Figure 10 shows the weight fraction crystallinity calculated from density (open symbol) and heat of fusion (filled symbol) and void content. The weight fraction crystallinity increased with the increase in draw ratio and with the rise in roller temperature. The roller-drawn homopolymer sheets showed the higher degree of crystallinity than the roller-drawn copolymer sheets. The crystallinity calculated from heat of fusion was lower than that from density and the difference was larger at lower draw ratio. This is because the heat of fusion is affected by the structural factors such as crystal thickness and number of chain folds on crystal surfaces.

The roller-drawn homopolymer sheet of λ = 4.5 contains a small amount of microvoids, which is formed in the destruction process of original spher-

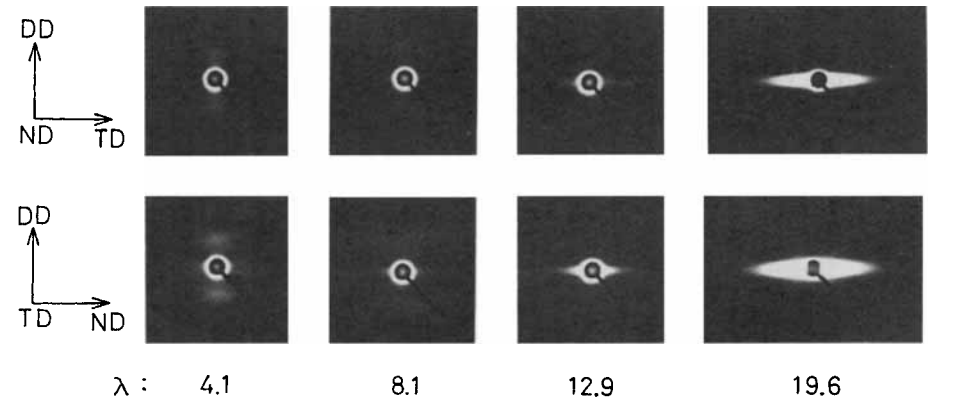

Fig. 9. SAXS patterns of roller-drawn POM copolymer sheets (T_r = 150°C).

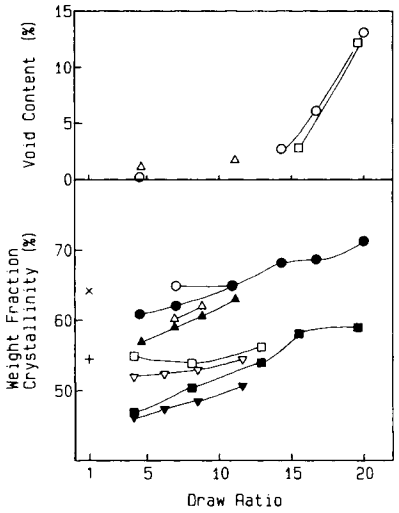

Fig. 10. Weight fraction crystallinity and void content vs. draw ratio: (△, ▲) homopolymer, T_r = 140°C; (○, ●) homopolymer, T_r = 157°C; (×) original homopolymer sheet; (▽, ▼) copolymer, T_r = 140°C; (□, ■) copolymer, T_r = 150°C; (+) original copolymer sheet: (×, +, △, ○, ▽, □) calculated from density; (▲, ●, ▼, ■) calculated from heat of fusion.

ulite structure. The microvoid content was reduced in the roller-drawn homopolymer sheets with intermediate draw ratio ($\lambda = 6-10$) and the roller-drawn copolymer sheets with draw ratio less than 14. The void content steeply increased with increasing draw ratio in the higher draw ratio range ($\lambda > 14$). The microvoids in the highly drawn sheets were formed in the interfibrillar region during the deformation process of fibrillar structure.

Long Period and Crystallite Size

The long period, L and the crystallite size, D_{100} are shown in Figure 11. The value of D_{100} decreased with increasing draw ratio in the lower draw ratio range, suggesting that the cleavage of crystallites occurred in the (100) plane at the initial stage of roller-drawing. The value of L tended to decrease slightly with increasing draw ratio and was larger at higher roller temperature.

The crystallite size, D_{001} and the relative fluctuation of the (001) planes, g are shown in Figure 12. The crystallite size, D_{001} increased monotonically with draw ratio, whereas only a small change with draw ratio was observed in the relative fluctuation of the (001) planes. The relative fluctuation of the (001) planes decreased and the crystalline order increased with the rise in roller temperature. The roller-drawn homopolymer sheets showed larger crystallite size, D_{001}, longer long period, and lower relative fluctuation of the (001) planes than the roller-drawn copolymer sheets.

Fracture Surface Morphology

Figure 13 shows draw ratio dependence of fracture surface morphology of roller-drawn copolymer sheets. Although the copolymer sheet of $\lambda = 4.1$ exhibited anisotropic feature, the fibrillar morphology was not fully developed at this stage. On the other hand, the well-oriented fibrillar structure

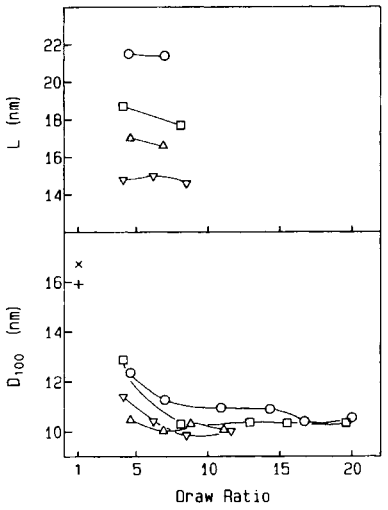

Fig. 11. Long period and crystallite size, D_{100} vs. draw ratio: (△) homopolymer, T_r = 140°C; (○) homopolymer, T_r = 157°C; (×) original homopolymer sheet; (▽) copolymer, T_r = 140°C; (□) copolymer, T_r = 150°C; (+) original copolymer sheet.

was observed in the fracture surface of the sheets of $\lambda = 8.1$ and $\lambda = 19.6$. With increasing draw ratio, the contact of fibrils became loose and microvoids were formed in the interfibrillar region.

Relationship Between Mechanical Properties and Structure

A spherulite structure having lamellar crystals is present in an original POM sheet.[27] The spherulite structure was transformed to the fibrillar one in the roller-drawing process. In the initial stage of roller drawing, lamellae break up into crystallite blocks, which are subsequently arranged to form

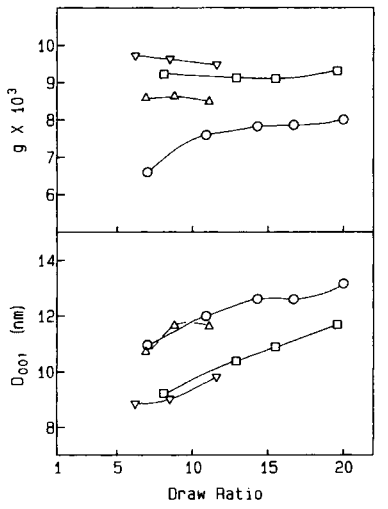

Fig. 12. Crystallite size, D_{001} and relative fluctuation of the (001) planes, g vs. draw ratio: (△) homopolymer, T_r = 140°C; (○) homopolymer, T_r = 157°C; (▽) copolymer, T_r = 140°C; (□) copolymer, T_r = 150°C.

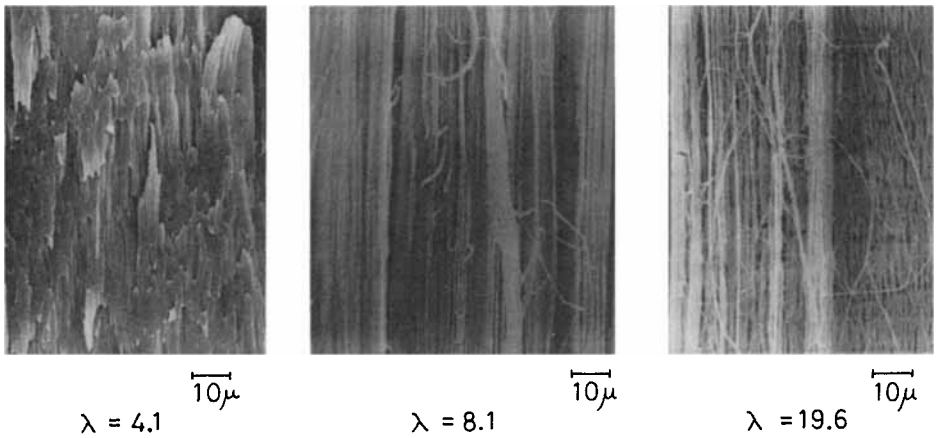

Fig. 13. Fracture surface morphology of roller-drawn POM copolymer sheets (T_r = 150°C): draw direction is vertical.

microfibrils. In this process, the crystallite size, D_{100} is much reduced and the crystal orientation function increased up to the maximum value. The transformation to the fibrillar structure is almost completed at the draw ratio of 7–8 (Fig. 13).

Peterlin proposed that amorphous taut tie molecules are formed in the interfibrillar and intercrystallite regions in the process of plastic deformation of polymeric materials.[28,29] The tie molecules increase in number and in tautness with increasing draw ratio. It was also reported that the tie molecules tended to crystallize into crystalline bridges in the case of hot drawing.[30,31]

The intensity of the meridional two-point SAXS decreased with increasing draw ratio and disappeared above $\lambda = 12$. The decrease in SAXS intensity suggests the increase in the density of intercrystallite region. Although the long period slightly decreased with increasing draw ratio, the crystallite size, D_{001} and the degree of crystallinity monotonically increased with draw ratio. The increase in D_{001} is attributable to the stress-induced crystallization of strained amorphous molecular chains. These changes in the noncrystalline region are reasonably explained by the concept of the formation of taut tie molecules and crystalline bridges. In the higher draw ratio range ($\lambda > 7$), the increase in the intercrystallite and interfibrillar links is the major structural change in the deformation process.

The taut tie molecules and the crystalline bridges would restrict the molecular motion of the amorphous region. The intensity of the γ-dispersion absorption peak decreased with increasing draw ratio. The depression of the γ-dispersion peak is interpreted as a result of the increase of these intercrystallite and interfibrillar links.

As the modulus of the amorphous region is much smaller than that of the crystalline region, the amorphous tie molecules and the crystalline bridges play a dominant role in the improvement of mechanical properties. The Young's modulus and the tensile strength are expected to increase with increasing the fraction of the intercrystallite and interfibrillar links. In the higher draw ratio range (λ = 14–20), however, the increase in the Young's

modulus is suppressed and the tensile strength decreases with increasing draw ratio (Fig. 1). As the fraction of microvoids greatly increases with draw ratio above $\lambda = 14$, the microvoids are considered to disturb the improvement of the mechanical properties.

If the crosssectional area of the roller-drawn sheets is corrected for microvoid content, the maximum Young's moduli of the roller-drawn homopolymer and copolymer sheets amount to 29.5 GPa and 21.8 GPa, respectively, at room temperature. These values are significantly higher than the Young's modulus at draw ratio of 12–15. The corrected value of dynamic storage modulus of the roller-drawn POM sheets approaches a value of 55 GPa at −150°C, which corresponds to the 52% of the crystal modulus (105 GPa).[32]

The microvoids have a more serious effect on the tensile strength than on the Young's modulus. The corrected tensile strength of the roller-drawn homopolymer sheet of $\lambda = 20$ is 0.88 GPa and is still lower than the tensile strength at $\lambda = 10$–15. The microvoids tend to disrupt the interfibrillar bonding during tensile tests, leading to the sample fracture at lower stress.

Comparison Between Roller-Drawn Homopolymer and Copolymer Sheets

The roller-drawn POM copolymer sheets exhibited much similarity to the roller-drawn homopolymer sheets in maximum draw ratio, tensile strength, crystal structure, crystal orientation, and lateral dimension of crystallite, D_{100}. In the POM copolymer sheet, the ethylene unit —CH_2—CH_2– is introduced in the main chain of polyoxymethylene sequence. The introduction of the ethylene unit restricts the crystallization of polyoxymethylene chains. Therefore, the degree of crystallinity of copolymer sheets is lower than that of the homopolymer sheets, which seems to have influence on the Young's modulus. The roller-drawn copolymer sheets show lower Young's modulus than the roller-drawn homopolymer sheets at the same draw ratio.

The value of long period and crystal thickness, D_{001} are smaller in the roller-drawn copolymer sheets compared with those in the roller-drawn homopolymer sheets of the similar draw ratio. The copolymer sheets exhibit the larger relative fluctuation of the (001) planes than the homopolymer sheets. It is evident that the crystalline order and crystal thickness are reduced by the copolymerization of the ethylene unit.

CONCLUSION

The high-modulus and high-strength POM sheets were shown to be produced by the roller-drawing process. The roller-drawing is applicable to thick polymer sheets, but has difficulty in producing wide sheets.

The spherulite structure in an original POM sheet is transformed to the fibrillar structure in the lower draw ratio range ($\lambda < 7$–8). The fibrillar structure is deformed accompanied by the increase in taut tie molecules and crystalline bridges at higher draw ratio ($\lambda > 7$–8). These structural changes play an important role in the improvement of the mechanical properties. In the higher draw ratio range ($\lambda > 15$), however, the formation

of interfibrillar microvoids restricts the improvement of mechanical properties.

The roller-drawn copolymer sheets show much similarity to the roller-drawn homopolymer sheets in tensile strength, crystal structure, crystal orientation, and lateral dimension of crystallite. The crystalline order, crystal thickness, D_{001}, and crystallinity are lower in the roller-drawn copolymer sheets than in the roller-drawn homopolymer sheets.

References

1. E. S. Clark and L. S. Scott, *Polym. Eng. Sci.*, **14**, 682 (1974).
2. B. Brew and I. M. Ward, *Polymer*, **19**, 1338 (1978).
3. D. M. Gezovich and P. H. Geil, *J. Mater. Sci.*, **6**, 509 (1971).
4. S. Bahadur, *Polym. J.*, **7**, 613 (1975).
5. K. Nakayama, K. Satake, T. Oki, and H. Kanetsuna, *J. Jpn. Soc. Tech. Plas.*, **15**, 744 (1974).
6. P. D. Coates and I. M. Ward, *J. Polym. Sci., Polym. Phys. Ed.*, **16**, 2031 (1978).
7. P. S. Hope, A. Richardson, and I. M. Ward, *J. Appl. Polym. Sci.*, **26**, 2879 (1981).
8. P. S. Hope, A. Richardson, and I. M. Ward, *Polym. Eng. Sci.*, **22**, 307 (1982).
9. K. Nakagawa, T. Konaka, and S. Yamakawa, *Polymer*, **26**, 84 (1985).
10. T. Konaka, K. Nakagawa, and S. Yamakawa, *Polymer*, **26**, 462 (1985).
11. A. Kaito, K. Nakayama, and H. Kanetsuna, *J. Appl. Polym. Sci.*, **30**, 1241 (1985).
12. A. Kaito, K. Nakayama, and H. Kanetsuna, *Kobunshi Ronbunshu*, **42**, 231 (1985).
13. A. Kaito, K. Nakayama, and H. Kanetsuna, *J. Appl. Polym. Sci.*, **30**, 4591 (1985).
14. P. H. Hermans, *Physics and Chemistry of Cellulose Fibres*, Elsevier, Amsterdam, 1949.
15. P. Scherrer, *Gött. Nachr.*, **2**, 98 (1918).
16. R. Hosemann and S. N. Bagchi, *Direct Analysis of Diffraction by Matter*, North-Holland, Amsterdam, 1962.
17. K. Nakayama, S. Okajima, and Y. Kobayashi, *J. Appl. Polym. Sci.*, **13**, 659 (1969).
18. P. G. Schmidt, *J. Polym. Sci.*, A, **1**, 1271 (1963).
19. H. Wilski, *Kolloid Z. Z. Polym.*, **248**, 867 (1971).
20. G. Carazzolo, *Gazz., Chim. Ital.*, **92**, 1345 (1962).
21. H. W. Starkweather and R. H. Boyd, *J. Phys. Chem.*, **64**, 410 (1960).
22. G. Carazzolo, *J. Polym. Sci., A*, **1**, 1573 (1963).
23. G. Carazzolo, M. Mammi, *J. Polym. Sci., A*, **1**, 965 (1963).
24. T. Uchida and H. Tadokoro, *J. Polym. Sci., A-2*, **5**, 63 (1967).
25. Y. Saruyama, H. Miyaji, and K. Asai, *J. Polym. Sci., Polym. Phys. Ed.*, **17**, 1163 (1979).
26. A. Kaito, K. Nakayama, and H. Kanetsuna, unpublished result.
27. C. F. Hammer, T. A. Koch, and J. F. Whiteney, *J. Appl. Polym. Sci.*, **1**, 169 (1959).
28. A. Peterlin, *J. Polym. Sci., A-2*, **7**, 1151 (1969).
29. A. Peterlin, *J. Mater. Sci.*, **6**, 490 (1971).
30. A. G. Gibson, G. R. Davies, and I. M. Ward, *Polymer*, **19**, 683 (1978).
31. A. Peterlin, *Polym. Eng. Sci.*, **18**, 488 (1978).
32. B. Brew, J. Clements, G. R. Davies, R. Jakeways, and I. M. Ward, *J. Polym. Sci., Polym. Phys. Ed.*, **17**, 351 (1979).

Received June 21, 1985
Accepted July 15, 1985